Clays and Clay Minerals, Vol. 47, No. 1, 1–11, 1999.

DESTINEZITE ("DIADOCHITE"), $Fe_2(PO_4)(SO_4)(OH)\cdot 6H_2O$: ITS CRYSTAL STRUCTURE AND ROLE AS A SOIL MINERAL AT ALUM CAVE BLUFF, TENNESSEE†

DONALD R. PEACOR,[1] ROLAND C. ROUSE,[1] T. DENNIS COSKREN[2] AND ERIC J. ESSENE[1]

[1] Department of Geological Sciences, University of Michigan, Ann Arbor, Michigan 48109, USA
[2] 6324 Sandchain Road, Columbia, Maryland 21045, USA

Abstract—A new occurrence of destinezite (diadochite), ideally $Fe_2(PO_4)(SO_4)(OH)\cdot 6H_2O$, is described from Alum Cave Bluff, Great Smoky Mountains National Park, Tennessee, where it occurs in soil and in a weathered Precambrian phyllite in unusually large crystals associated with other hydrated sulfates such as pickeringite–apjohnite. Destinezite is triclinic, $P\bar{1}$, with a = 9.570(1), b = 9.716(1), c = 7.313(1) Å, α = 98.74(1)°, β = 107.90(1)°, γ = 63.86(1)° and Z = 2. Its crystal structure consists of infinite chains of $Fe(O,OH,H_2O)_6$ octahedra, sulfate tetrahedra and phosphate tetrahedra linked by a unique system of vertex sharing. The chains are weakly bonded into slabs by hydrogen bonding between OH and H_2O of the Fe(III) octahedra and oxygen ions of the sulfate tetrahedra. Slabs of tetrahedral/octahedral chains alternate with sheets of H_2O molecules. The structure thus somewhat resembles hydrated clay minerals, with H_2O molecules that act as hydrogen bond donors and acceptors to oxygen atoms of adjacent slabs. Destinezite and diadochite occur at numerous localities worldwide and have been assumed to be identical, but this identity has never been proven. It is proposed that the name "destinezite" be applied to visibly crystalline, triclinic $Fe_2(PO_4)(SO_4)(OH)\cdot 6H_2O$ and "diadochite" to massive to earthy, poorly ordered, X-ray amorphous materials that approximate destinezite in composition. Diadochite/destinezite may be an unrecognized component of soils where weathering of pyrite and apatite has occurred and pH is low. It may thus be a significant sink for phosphorus and sulfur in such soils.

Key Words—Crystal Structure, Destinezite, Diadochite, Phosphate-Sulphate, Soil Mineral.

INTRODUCTION

Diadochite and destinezite have variously been regarded as separate mineral species or as 2 forms of the same species, with destinezite being, in the words of Palache et al. (1951), "a mineral now known to be only a relatively coarsely crystalline variety of diadochite (a metacolloid in its original occurrences); diadochite has priority and is here used as the species designation." This latter view is commonly accepted in contemporary mineralogical reference works (Clark 1993; Fleischer and Mandarino 1995), even though the identity of diadochite and destinezite has never actually been demonstrated. The difficulty here is that, whereas destinezite is well crystallized and hence well characterized chemically, optically, and crystallographically, diadochite is amorphous (or very nearly so) to X-ray diffraction (XRD) and commonly shows a pronounced variation in chemical composition from one locality to another or even among specimens from the same locality (Hintze 1933; Jarkovský and Čícel 1958; Földvári and Nagy 1985).

Our interest in these relations derives from the discovery of destinezite crystals of unusually large size (up to 100 μm) occurring as a common constituent of the soil at a hitherto unreported locality, Alum Cave Bluff, Great Smoky Mountains National Park, Tennessee (Coskren and Lauf 1996). Their identification as destinezite was originally confirmed by powder XRD (G. W. Robinson, personal communication 1995). Using one such crystal, we have determined the crystal structure of destinezite, the details of which are reported here. To verify the identity of our material and destinezite, we have obtained destinezite from the type locality (Argenteau, near Visé, Belgium) and confirmed that their powder XRD patterns are essentially identical. The destinezite sample was obtained through the courtesy of Prof. A.-M. Fransolet of the University of Liège, Belgium, and is a fragment of the same specimen investigated by Cesàro (1885) in his definitive chemical and morphological study of this mineral (A.-M. Fransolet, personal communication 1995).

In addition to clarifying the distinction between destinezite and diadochite, this study calls attention to 2 new facts of interest to soil scientists, namely that destinezite should be added to the existing list of soil minerals and that destinezite and diadochite (especially the latter) may be significant components of soils formed under favorable geochemical conditions. The nature of those conditions will be described in a subsequent section of this report.

OCCURRENCE

The destinezite samples used in this study were collected from the soil and weathered bedrock at Alum

† Contribution No. 506. The Mineralogical Laboratory, Department of Geological Sciences, The University of Michigan, Ann Arbor, Michigan 48109, USA.

Figure 1. Euhedral crystals of destinezite associated with acicular gypsum from Alum Cave Bluff.

Cave Bluff, on the slope of Mount Le Conte in the Great Smoky Mountains, Sevier County, Tennessee. The minerals have been studied extensively by Coskren and Lauf and are the subject of a previous, brief report (Coskren and Lauf 1996). Minerals present in the soil under an overhanging cliff are predominantly epsomite and pickeringite–apjohnite solid solutions, but there are also a variety of other minerals, which are primarily hydrated sulfates. Among the less common minerals are 3 new hydrated REE sulfate-oxalates. All of these minerals owe their existence to weathering of up-slope bedrock consisting of pyrite-rich phyllites of the Precambrian Anakeesta Formation. Surface runoff transports weathering products down to the overhanging cliff. Despite a high rainfall of over 60 inches per year in the surrounding area, the environment under the cliff overhang is dry, resulting in evaporation of surface runoff and precipitation of water-soluble compounds. Most of the minerals present in the soil are highly soluble hydrates, whose origin is related to the locally wet conditions. Destinezite, however, is much less soluble than most of its associated minerals. It should therefore be more robust than its associates, and we infer that it should occur in less arid situations.

Destinezite occurs in 2 closely related associations at Alum Cave Bluff. The first consists of euhedral crystals approximately 30 μm in size on surfaces and in crevices of partially altered phyllite bedrock, where it is commonly associated with gypsum crystals (Figure 1). The destinezite is present as pulverulent buff to salmon-colored masses and coatings on rock fragments, and as isolated crystals on acicular gypsum crystals up to a few mm in length. The second type of occurrence is as larger crystals up to 100 μm in size embedded within massive pickeringite–apjohnite or in crystal cavities of the latter.

Table 1. Crystal data for destinezite.

Alum Cave Bluff, Great Smoky Mts.†		
Triclinic—$P\bar{1}$		
a = 9.570 (1)	b = 9.716 (1)	c = 7.313 (1) Å
α = 98.74 (1)°	β = 107.90 (1)°	γ = 63.86 (1)°
V = 580.8 (2) Å^3		
$(Fe_{1.77}Al_{0.23})(PO_4)(SO_4)(OH)\cdot 6H_2O$		Z = 2
ρ(calc) = 2.411 g/cm^3		
Haut-le-Wastia, Belgium‡		
Triclinic (alternative unit cell)		
a = 9.585 (1)	b = 10.235 (1)	c = 7.335 (1) Å
α = 81°46 (1)′	β = 107°57 (1)′	γ = 121°10 (1)′
V = 585.7 (1) Å^3		
$Fe_{2.00}(PO_4)_{1.00}(SO_4)_{0.91}(OH)\cdot 5.8H_2O$		Z = 2
ρ(obs) = 2.27 g/cm^3 (Hintze 1933)		

† All data are derived from the crystal-structure analysis (this study).

‡ Cell parameters are from powder diffractometer data and the formula is from a wet-chemical analysis (Van Tassel 1985). The density is for crystals from Védrin, Belgium (Hintze 1933).

X-RAY CRYSTALLOGRAPHY

Euhedral crystals of destinezite from the new locality were separated from their associated minerals under a binocular microscope on the basis of their color and morphology. This identification was confirmed by a Gandolfi photograph, the data from which accorded well with PDF 12-209, 24-528 and 42-1364 ("diadochite" on the PDF cards). After a preliminary study with the precession camera, which confirmed the triclinic symmetry of destinezite reported by Larsen (1921), the best-quality crystal was mounted on an Enraf-Nonius CAD4 4-circle diffractometer, and its unit-cell parameters were refined by least-squares from the optimized setting angles of 25 reflections between 18 and 33° 2θ. The unit-cell orientation given on PDF 42-1364 was used throughout the course of this study. Table 1 summarizes the basic crystal-chemical data of Alum Cave Bluff destinezite and, for comparison, the same data for destinezite from Haut-le-Wastia, Belgium (Van Tassel 1985). The latter uses the other commonly used cell orientation for this mineral.

CHEMICAL COMPOSITION

A polished thin-section of Alum Cave Bluff destinezite was prepared by setting in resin, dry cutting and then polishing without the use of water. Although the resin was not heated, exothermic processes that occurred during setting may have caused some heating of the sample. In thin-section, curved fractures were observed in the crystals, a feature that implies some degree of thermal dehydration of the sample during preparation. Wavelength-dispersive scans with a Cameca CAMEBAX electron microprobe (EMP) confirmed the absence of As at the 0.1 wt% level and the presence of Mg in the crystals; that is, the Mg content

https://doi.org/10.1346/CCMN.1999.0470101 Published online by Cambridge University Press

Table 2. Selected chemical analyses of destinezite (wt%).†

	1	2	3	4	5	6	7§	8	9	10
CaO					0.19	0.80				
MgO							0.3			
FeO			0.07							
Fe_2O_3	37.33	37.60	37.80	36.20	37.66	35.60	36.2	38.72	37.84	35.71
Al_2O_3							2.7	0.72		
P_2O_5	16.59	16.76	16.83	17.20	16.50	18.50	17.1	15.92	15.95	19.92
As_2O_5									1.39	
V_2O_5										0.11
SiO_2						0.56				
SO_3	18.71	18.85	17.21	19.50	19.32	17.30	20.7	19.16	18.80	19.49
H_2O^+			16.76			18.30		24.68	17.60	
H_2O^-			10.04			8.00		—	8.96	
H_2O (total)	27.37	25.65	26.80	26.90‡	26.47	26.30	(23.0)¶	24.68	26.56	(24.77)¶
Rem.		1.40	0.86		0.04	1.00		0.69		
Sum	100.00	100.26	99.57	99.80	100.18	100.06	(100.0)	99.89	100.54	(100.00)

† Localities: 1—Theoretical for $Fe_4(PO_4)_2(SO_4)_2(OH)_2{\cdot}12H_2O$. 2—Argenteau, Belgium (type locality) (Cesàro 1885). 3—Haut-le-Wastia, Namur, Belgium (Van Tassel 1985). 4—Saryjas, Kygyzstan (Ankinovich 1958). 5—Chvaletice, Bohemia (Veselý 1922). 6—Northwest Kara Tau, Kazakhstan (Ankinovich 1958). 7—Alum Cave Bluff, Great Smoky Mountains, Tennessee (this study). 8—Kurama Ridge, Tokmak, Uzbekistan (Moiseeva 1967). 9—Blyava, Southern Urals, Russia (German 1956). 10—Roberts Mountain, near Eureka, Nevada (Hausen 1962).

‡ Given as "29.90" in Ankinovich (1958), but 26.90 is consistent with the stated sum of "99.80" and with the water content of destinezite from other localities.

§ Sample slightly dehydrated during preparation and EMP analysis.

¶ Water determined by difference.

of this destinezite is not due to inclusions of a second phase. A preliminary examination with successive 10-s analytical intervals revealed that the mineral was sensitive to the electron beam, with a monotonic increase in S, P and Fe concentrations with time. Presumably this was due to partial dehydration of the crystals under the beam. Therefore, the sample was analyzed with a low beam current (6 nA), a relatively wide scanning beam (6 × 6 μm raster) on both standards and sample, short counting times (10 s) and an averaging of the 10 analyses performed. The resulting average analysis (analysis 7 in Table 2) has Fe_2O_3 ($+Al_2O_3$), P_2O_5 and SO_3 concentrations that exceed the theoretical values for $Fe_2(PO_4)(SO_4)(OH){\cdot}6H_2O$, confirming that some dehydration did occur during sample preparation and/or microprobe analysis.

Table 2 compares the composition of Alum Cave Bluff destinezite with those of the same mineral from a representative selection of localities and parageneses reported in the literature. Care was taken to consult the original publications to ensure that the reported analyses were actually performed on well-crystallized destinezite rather than on diadochite. The analyses in Table 2 demonstrate that, unlike diadochite, the chemical composition of destinezite varies only within narrow limits and is essentially constant when minor cation substitutions are taken into account. The nature of those substitutions is evident from Table 3, which contains the unit-cell contents for each analysis in Table 2 calculated using the measured cell volume and calculated density of the Alum Cave Bluff material (Table 1). Analysis 7 implies solid solution of Fe(III) and

Table 3. Unit-cell contents from analyses in Table 2.†

	1	2	3	4	5	6	7	8	9	10
Ca					0.03	0.12				
Mg							0.06			
Fe^{II}			0.01							
Fe^{III}	4	3.97	3.99	3.82	3.98	3.76	3.82	4.09	4.00	3.77
Al							0.45	0.12		
P	2	1.99	1.99	2.04	1.96	2.20	2.03	1.89	1.90	2.37
As									0.10	
V										0.01
Si						0.11				
S	2	1.99	1.81	2.05	2.03	1.82	2.18	2.02	1.98	2.05
H	26	24.02	25.09	25.18	24.78	24.62	21.54	23.10	24.87	23.20
O	30	28.90	28.97	29.60	29.39	29.25	28.86	28.65	29.36	29.37
H_2O	12	11.01	11.54	11.59	11.39	11.31	(9.77)	10.55	11.43	(10.60)

† Calculated using the unit-cell volume and calculated density of Alum Cave Bluff destinezite.

https://doi.org/10.1346/CCMN.1999.0470101 Published online by Cambridge University Press

Table 4. Experimental details.

Crystal size	0.055 × 0.047 × 0.031 mm
Radiation	Monochromatized Mo$K\alpha$, 50 kV and 30 mA
Data measurement	
Index limits	$-12 \leq h,k \leq 12$ and $0 \leq l \leq 9$
Maximum 2θ	54.90°
Scan type	ω/2θ
Scan rates	Between 0.4° and 5.5°/min in ω
Scan widths	0.78 + 0.35 tan θ
Intensity monitoring	3 reflections every 3 h
Orientation monitoring	3 reflections every 400 reflections
Data corrections	Lorentz-polarization and absorption (μ_l = 26.5 cm^{-1})
Structure refinement	
Type	Full-matrix least-squares
Function minimized	$\Sigma w(\|F\|_{obs}-\|F\|_{cal})^2$
Reflection weights	$4F^2_{obs}/\sigma^2$ (F^2_{obs})
Anomalous dispersion	For all atoms
Observations	1420 reflections with $I > 2\sigma(I)$
Variables	174
R (observed data)	0.046
wR_w (observed data)	0.048
R (all data)	0.182
Esd obs. of unit wt.	1.22
Largest shift/error	0.00
Largest Δρ (x, y, z)	+0.75 and −0.29 e/Å^3
Diffractometer	Enraf-Nonius CAD4
Computation	
Hardware	MicroVAX 3100
Software	MolEN system

Table 6. Positional and equivalent isotropic displacement parameters (Å^2).

Atom	x	y	z	B (Å^2)
M1	0.8951 (1)	0.3128 (1)	0.8005 (1)	0.97 (2)
M2	0.2380 (1)	0.2948 (1)	0.6822 (1)	0.91 (2)
P	0.0544 (2)	0.3842 (2)	0.2426 (2)	0.94 (4)
S	0.7016 (2)	0.2353 (2)	0.3769 (2)	1.35 (4)
O1w	0.3408 (5)	0.2869 (6)	0.9787 (7)	1.9 (1)
O2	0.7363 (5)	0.3479 (5)	0.5281 (7)	1.6 (1)
O3	0.0260 (5)	0.2823 (5)	0.0691 (6)	1.4 (1)
O4w	0.4052 (5)	0.3673 (5)	0.6493 (7)	1.6 (1)
O5w	0.9092 (5)	0.0942 (5)	0.7935 (7)	1.8 (1)
O6	0.1673 (5)	0.2773 (5)	0.4078 (6)	1.4 (1)
O7h	0.0866 (5)	0.2194 (5)	0.7057 (6)	1.4 (1)
O8	0.8625 (5)	0.5246 (5)	0.7987 (7)	1.6 (1)
O9	0.1041 (5)	0.5077 (5)	0.7138 (6)	1.5 (1)
O10w	0.6937 (5)	0.3772 (5)	0.8963 (6)	1.6 (1)
O11w	0.7226 (6)	0.0121 (6)	0.9289 (8)	2.5 (1)
O12	0.6188 (6)	0.3181 (6)	0.1953 (7)	2.3 (1)
O13w	0.4221 (5)	0.0824 (5)	0.6852 (7)	1.9 (1)
O14	0.4044 (5)	0.8136 (5)	0.5710 (7)	2.0 (1)
O15	0.1490 (6)	0.8936 (7)	0.6358 (8)	3.3 (2)
H1	0.4186	0.3127	0.0234	4.7
H2	0.2500	0.3610	0.0014	4.7
H3	0.3625	0.4384	0.5725	4.7
H4	0.4548	0.3114	0.5731	4.7
H5	0.0181	0.9930	0.2502	4.7
H6	0.1648	0.9375	0.2017	4.7
H7	0.0931	0.1308	0.6328	4.7
H8	0.3334	0.6197	0.9963	4.7
H9	0.2869	0.5306	0.1136	4.7
H10	0.2969	0.9115	0.9752	4.7
H11	0.2316	0.0852	0.0617	4.7
H12	0.4766	0.9426	0.2518	4.7
H13	0.4142	0.9896	0.6657	4.7

Note: Anisotropically refined atoms are given with their isotropic equivalent displacement parameters, defined as $4/3[a^2B(1,1) + b^2B(2,2 + c^2B(3,3) + ab(\cos\gamma)B(1,2) + ac(\cos\beta)B(1,3) + bc(\cos\alpha)B(2,3)]$. Esds are in parentheses. The H atoms were held constant at the coordinates derived from the difference synthesis and B_{iso} values of 4.7 Å^2.

Al(III) on the octahedral sites of destinezite, and this is confirmed by the crystal-structure analysis, which yielded ($Fe_{3.54}Al_{0.46}$) per cell. By contrast, analysis 8 is consistent with full occupancy of the octahedral sites by 4 Fe and with ($P_{1.9}Al_{0.1}$) on the tetrahedral P site. Analysis 9 implies a different substitution for P, namely ($P_{1.9}As_{0.1}$). The only possible substitutions indicated for the tetrahedral S site are ($S_{1.8}P_{0.2}$) or ($S_{1.8}Si_{0.1}$) in analysis 6. The former is possible, but the Si in analysis 6 is probably a contaminant, microcrystalline silica being sometimes associated with destinezite. Analysis 10 shows minor V, but its structural role is ambiguous owing to the quality of the analysis. Both [Fe(III), V(III)] and [P(V), V(V)] solid solutions are possible based on ionic charge and radius considerations.

Many analyses of destinezite show minor CaO and MgO, for example, analyses 5–7. These components have usually been attributed to sample contamination, but the EMP results presented here show that this may not always be the case. Modern analyses of diadochite (such as Földvári and Nagy 1985) show numerous additional minor and trace components such as K_2O, Na_2O, MnO, PbO, TiO_2 and CO_2, but this is merely a reflection of the general variability and uncertainty in the composition of that mineral. Table 3 also indicates that the number of H_2O molecules in destinezite is between 11 and 12 per cell, discounting analyses 7 and 10 in which no analytical determination of H_2O was made. This is in accord with the crystal-structure analysis, which unambiguously indicates 12 H_2O per cell. The conventional formula of destinezite/diadochite, $Fe_2(PO_4)(SO_4)(OH)\cdot 5H_2O$ with $Z = 2$, given in mineralogical reference books is therefore in error in this respect.

STRUCTURE SOLUTION AND REFINEMENT

A total of 2874 reflection intensities in 1 asymmetric unit to a maximum 2θ of 55° were measured with a CAD4 diffractometer, and the data were corrected for Lorentz-polarization and absorption effects. The latter was done using the psi-scan method of North et al. (1968). Averaging of symmetry-equivalents yielded a final data set of 2664 reflections of which 1420 having $I > 2\sigma$ (I) were considered "observed." Additional details of the data measurement and reduction are presented in Table 4.

https://doi.org/10.1346/CCMN.1999.0470101 Published online by Cambridge University Press

Table 7. Anisotropic displacement parameters (Å²).

Atom	$U(1, 1)$	$U(2, 2)$	$U(3, 3)$	$U(1, 2)$	$U(1, 3)$	$U(2, 3)$
M1	0.0125 (3)	0.0148 (4)	0.0115 (4)	−0.0075 (3)	0.0025 (3)	0.0009 (3)
M2	0.0110 (3)	0.0123 (4)	0.0115 (4)	−0.0048 (3)	0.0028 (3)	0.0014 (3)
P	0.0128 (6)	0.0119 (7)	0.0100 (7)	−0.0044 (5)	0.0025 (5)	0.0015 (6)
S	0.0185 (6)	0.0169 (7)	0.0174 (8)	−0.0085 (5)	0.0074 (6)	−0.0045 (6)
O1w	0.017 (2)	0.029 (2)	0.024 (2)	−0.009 (2)	0.003 (2)	0.002 (2)
O2	0.021 (2)	0.021 (2)	0.018 (2)	−0.011 (1)	−0.001 (2)	0.005 (2)
O3	0.021 (2)	0.013 (2)	0.017 (2)	−0.004 (1)	0.006 (2)	−0.002 (2)
O4w	0.023 (2)	0.015 (2)	0.023 (2)	−0.009 (1)	0.009 (2)	−0.003 (2)
O5w	0.026 (2)	0.016 (2)	0.030 (2)	−0.009 (2)	0.011 (2)	−0.000 (2)
O6	0.018 (2)	0.015 (2)	0.013 (2)	−0.000 (2)	0.003 (2)	0.003 (2)
O7h	0.022 (2)	0.016 (2)	0.021 (2)	−0.010 (1)	0.011 (2)	−0.005 (2)
O8	0.019 (2)	0.020 (2)	0.022 (2)	−0.009 (1)	0.006 (2)	0.003 (2)
O9	0.018 (2)	0.019 (2)	0.019 (2)	−0.007 (1)	0.007 (2)	−0.000 (2)
O10w	0.021 (2)	0.025 (2)	0.021 (2)	−0.015 (1)	0.011 (2)	−0.002 (2)
O11w	0.030 (2)	0.024 (3)	0.037 (3)	−0.009 (2)	0.009 (2)	−0.002 (2)
O12	0.033 (2)	0.046 (3)	0.018 (2)	−0.026 (2)	−0.001 (2)	0.008 (2)
O13w	0.021 (2)	0.016 (2)	0.028 (3)	−0.006 (2)	0.000 (2)	0.001 (2)
O14	0.032 (2)	0.022 (2)	0.033 (3)	−0.019 (1)	0.013 (2)	−0.004 (2)
O15	0.028 (2)	0.040 (3)	0.048 (3)	−0.001 (2)	0.022 (2)	−0.009 (3)

Note: The form of the anisotropic displacement parameter is $\exp[-2\pi^2\{h^2a^2U(1, 1) + k^2b^2U(2, 2) + l^2c^2U(3, 3) + 2hkabU(1, 2) + 2hlacU(1, 3) + 2klbcU(2, 3)\}]$, where a, b and c are reciprocal lattice constants.

The structure was solved in space group $P\bar{1}$ using the direct methods program MULTAN11/82, which is incorporated in the Enraf-Nonius crystallographic software system MolEN. MULTAN revealed the locations of all cation sites (other than H) and 12 of the 15 anion sites. A difference synthesis revealed the remaining anion sites, and this model refined to an R(obs) of 8.6%, using isotropic displacement factors and unit weights for the reflections. Introduction of a weighting scheme based on $\sigma(F)$ and refinement of site occupancy factors for M1 and M2, assuming (Fe,Al) on each, reduced the unweighted R(obs) to 8.1%. Conversion to anisotropic displacement factors for all atoms reduced R(obs) to 5.7%, but the excessively elongated shapes of many of the ellipsoids indicated that the psi-scan absorption correction was inadequate. A supplementary absorption correction was therefore applied using the program DIFABS (Walker and Stuart 1983). This produced ellipsoids of reasonable shape and reduced R(obs) to 4.9%.

At this point, empirical bond-valence calculations identified O1w, O4w, O5w, O10w, O11w and O13w as belonging to H_2O molecules and O7h as part of the hydroxyl ion. A series of difference syntheses, combined with the application of the bond distance and angle criteria expected for H_2O in crystalline hydrates (Chiari and Ferraris 1982), revealed the probable positions of all 13 nonequivalent H atoms. However, the isotropic displacement factors of a few of these refined to negative values and their refined coordinates yielded H_2O bond parameters that were much less reasonable than those calculated from the coordinates derived from the difference synthesis. Accordingly, in the final cycles of refinement, the H coordinates were fixed at those from the difference maps and the H displacement factors were fixed at the average of the non-negative refined values, resulting in a final R(obs) of 4.6%. A final refinement of M1 and M2 site occupancy factors yielded 1.812(9) Fe + 0.188 Al and 1.733(9) Fe + 0.267 Al atoms, respectively. Additional details of the structure solution and refinement are presented in Table 4. Table 5 (a copy of Table 5 may be obtained by contacting the authors) contains the observed and calculated structure factors, Table 6 the refined atomic parameters, Table 7 the refined anisotropic atomic displacement factors and Table 8 some selected interatomic distances and angles.

DESCRIPTION OF CRYSTAL STRUCTURE

Overview of Structure Topology

Figure 2 is a plot of the structure projected parallel to c^* [onto (001)], whereas Figure 3 is a view in which the structure is rotated 90° around a [a view projected onto a plane near (010)]. The structure is dominated by chains extending infinitely parallel to c, viewed end-on in Figure 2 and perpendicular to their length in Figure 3. However, as shown in Figure 3, neighboring chains linked together by hydrogen bonds define slabs oriented parallel to (010), and these slabs are separated by single layers of water molecules, O11w. In that respect, the structure bears some resemblance to the hydrated layer silicates, although there is no evidence for expendability. Indeed, the system of hydrogen bonds that is described below appears to define a well-ordered structure in which the "interlayer" water, O11w, is essential in the defined stoichiometric formula.

Figures 4 and 5 show details of the chain, as projected approximately onto (100), that is, approximately

https://doi.org/10.1346/CCMN.1999.0470101 Published online by Cambridge University Press

Table 8. Selected interatomic distances (Å) and angles (°).

		$M(O, OH, H_2O)_6$ Octahedra			
	M1-O8	1.942 (6)		M2-O9	1.917 (5)
	O7h	1.946 (5)		O6	1.917 (5)
	O3	1.963 (5)		O7h	1.947 (5)
	O10w	2.057 (5)		O13w	2.037 (6)
	O5w	2.061 (6)		O1w	2.085 (6)
	O2	2.069 (5)		O4w	2.096 (5)
	Mean	2.006		Mean	2.000
		TO_4 Tetrahedra			
	P-O6	1.515 (5)		O3-P-O6	106.2 (3)
	O9	1.516 (5)		O3-P-O8	108.8 (3)
	O3	1.519 (5)		O6-P-O8	109.4 (3)
	O8	1.536 (6)		O8-P-O9	110.3 (3)
	Mean	1.522		O3-P-O9	110.6 (3)
				O6-P-O9	111.3 (3)
				Mean	109.4
	S-O15	1.446 (6)		O2-S-O12	106.5 (3)
	O14	1.455 (6)		O2-S-O14	107.9 (3)
	O12	1.468 (6)		O2-S-O15	110.0 (4)
	O2	1.502 (6)		O12-S-O14	110.3 (4)
	Mean	1.468		O12-S-O15	110.8 (4)
				O14-S-O15	111.2 (4)
				Mean	109.4
		H-Ow-H		Ow-H···O	
O1w		O1w-H1	0.84	H1···O12	1.96
		O1w-H2	0.90	O1w-H1···O12	159°
		H1-H2	1.43	H2···O8	1.99
		H1-O1w-H2	110°	O1w-H2···O8	146°
O4w		O4w-H3	0.83	H3···O2	2.01
		O4w-H4	0.82	O4w-H3···O2	160°
		H3-H4	1.16	H4···O14	1.86
		H3-O4w-H4	89°	O4w-H4···O14	171°
O5w		O5w-H5	0.92	H5···O15	1.86
		O5w-H6	0.90	O5w-H5···O15	156°
		H5-H6	1.40	H6···O11w	1.88
		H5-O5w-H6	101°	O5w-H6···O11w	153°
O7h		O7h-H7	0.93	H7···O15	2.13
				O7h-H7···O15	146°
O10w		O10w-H8	0.89	H8···O12	1.85
		O10w-H9	1.01	O10w-H8···O12	160°
		H8-H9	1.58	H9···O1w	2.32
		H8-O10w-H9	112°	O10w-H9···O1w	139°
O11w		O11w-H10	0.94	H10···O12	2.32
		O11w-H11	0.85	O11w-H10···O12	165°
		H10-H11	1.62	H11···O3	2.06
		H10-O11w-H11	130°	O11w-H11···O3	146°
O13w		O13w-H12	0.87	H12···O11w	1.86
		O13w-H13	0.92	O13w-H12···O11w	168°
		H12-H13	1.41	H13···O14	1.78
		H12-O13w-H13	103°	O13w-H13···O14	166°
			Ow-O		
O1w	O1w-O12	2.766 (8)	O10w	O10w-O12	2.707 (7)
	O8	2.773 (8)		O1w	3.149 (8)
O4w	O4w-O2	2.807 (7)	O11w	O11w-O12	3.232 (9)
	O14	2.669 (8)		O3	2.811 (8)
O5w	O5w-O15	2.720 (8)	O13w	O13w-O11w	2.721 (8)
	O11w	2.717 (8)		O14	2.680 (8)
O7h	O7h-O15	2.944 (9)			

parallel to *a*, so that the chain direction, *c*, is horizontal, and the view of the chain is from the side. The repeating subunit of the chain consists of 2 MX_6 octahedra [M = (Fe,Al) and X = (O,OH,H_2O)] and a PO_4 tetrahedron. $M(1)X_6$ and $M(2)X_6$ octahedra share a common vertex, and the PO_4 tetrahedron shares 1 vertex each with the 2 kinds of octahedra, forming a 3-membered polyhedral ring. As shown in Figure 5, such units are staggered and are linked along the chains' length by sharing tetrahedral vertices. The arrangement is one in which each phosphate tetrahedron shares all 4 of its vertices with $M(1)X_6$ and $M(2)X_6$ octahedra, knitting the chain together, but from within the body of the chain. By contrast (Figure 2), each SO_4 tetrahedron is attached to the chain along its periphery, sharing 1 vertex with an $M(1)X_6$ octahedron and with 2 other vertices pointing towards an adjacent chain.

Süsse (1971) has suggested a simple way to diagram the linkages between tetrahedra and octahedra in related structures that have infinitely extended chains consisting of vertex-sharing octahedra and tetrahedra. Figure 6 shows such diagrams for destinezite and for several other sulfates having related types of chains. The topology of the chain in destinezite appears to be unique, based on our review of such relations in other sulfate and phosphate structures. Members of the butlerite–fibroferrite group (Mereiter 1979; Scordari 1981), botryogen (Süsse 1968) and copiapite (Süsse 1972) all contain chains made up of the same 3-membered-ring subunits that occur in destinezite, but the method of linking subunits is different in each case (Figure 6).

Hydrogen Bonding

Empirical bond valences (Table 9) fall into the well-defined ranges expected for oxide ions, hydroxyl ions and water molecules. The bond valence sums are approximately 0.4 for O1w, 04w, O5w, O10w and O13w, consistent with a slight overbonding of the water molecules that are bonded to M1 and M2. However, the valence sum to O11w is zero, consistent with its role as an interlayer molecule not bonded to any cation. The sum of 1.17 defines O7h as a hydroxyl ion. The oxide ions are all underbonded, with sums less than 2.00. Valence sums for O of phosphate tetrahedra are in the range 1.80 to 1.90, consistent with a slight underbonding. Three of the 4 O atoms of the sulfate tetrahedra, O12, O14 and O15, are severely underbonded, with sums of 1.52 to 1.62, owing to the fact that they are unshared tetrahedral vertices. A need for valence contributions from several H bonds is therefore indicated for each of these atoms.

Hydrogen bonding serves 2 purposes in the destinezite structure: 1) From the viewpoint of structural topology, it provides the only linkage between adjacent tetrahedral-octahedral chains. As shown in Fig-

https://doi.org/10.1346/CCMN.1999.0470101 Published online by Cambridge University Press

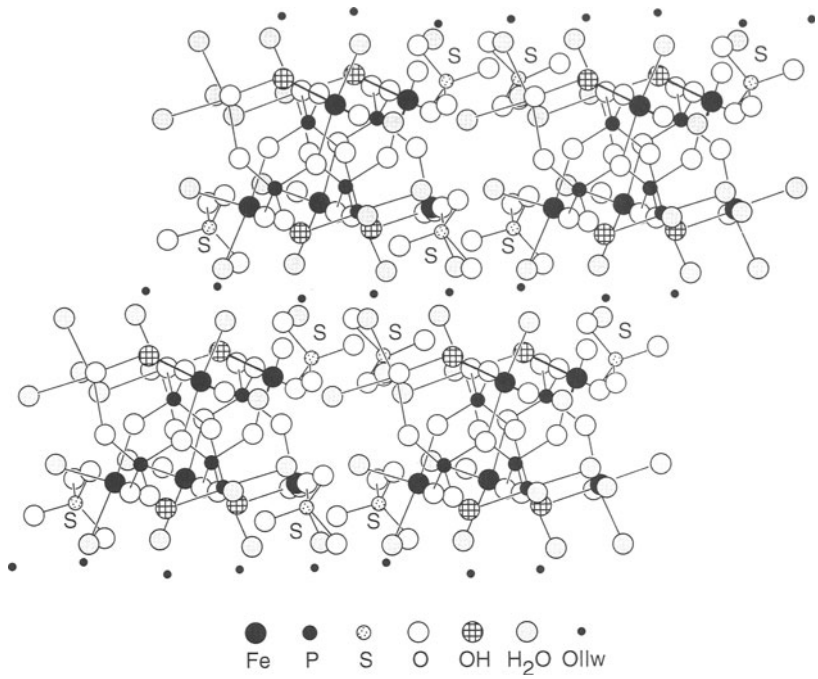

Figure 2. A projection of the structure onto (001), showing end-on views of 4 chains. The chains are linked together in the horizontal direction by hydrogen bonds to form slabs parallel to (010). The slabs are separated from one another in the vertical direction by single sheets of "interlayer" H_2O molecules (O11w), represented here as black dots.

ures 3 and 4, the sulfate tetrahedra, which are situated on the periphery of the chains, are adjacent to octahedron vertices defined by hydroxyl ions and water molecules. These 2 groups serve as charge donors and the oxygen atoms of sulfate groups as receptors, bonding parallel chains into slabs oriented parallel to (010). 2) From a charge distribution viewpoint, H-bonding effectively redistributes electronic charge throughout the structure, especially from the overbonded oxygen atoms of the H_2O and OH groups to the severely underbonded oxygen atoms of the sulfate groups and the moderately underbonded phosphate oxygen atoms.

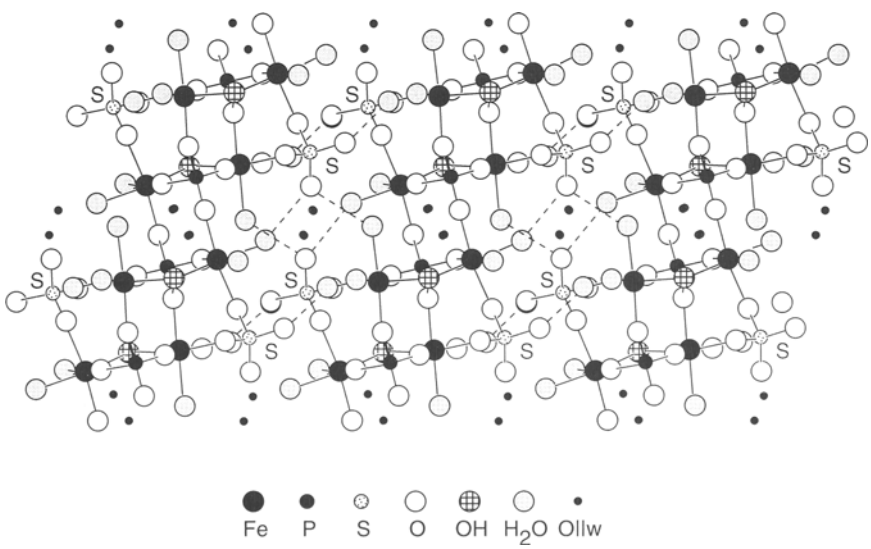

Figure 3. A projection of 3 chains from 1 of the slabs in Figure 2 onto a plane near (010), that is, a top view of part of 1 slab. The interchain gaps are bridged in the horizontal direction by hydrogen bonds (dashed lines) between the $M(O,OH,H_2O)_6$ octahedra in 1 chain and the SO_4 tetrahedra in the adjacent chain. All chains thus linked constitute 1 slab.

https://doi.org/10.1346/CCMN.1999.0470101 Published online by Cambridge University Press

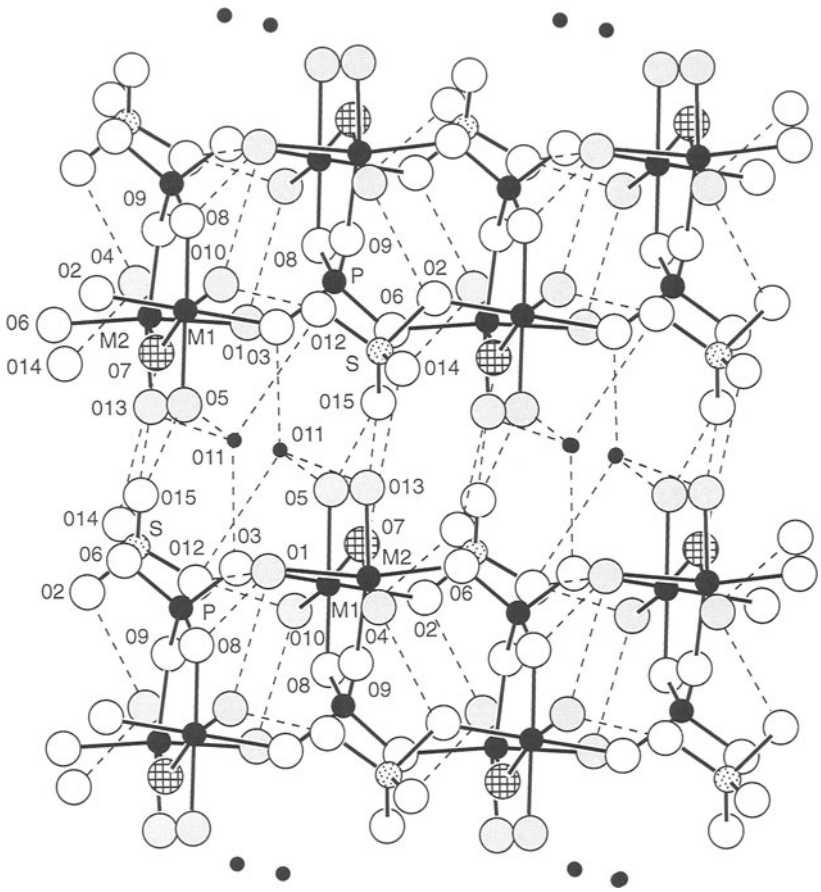

Figure 4. A projection of 2 chains onto a plane near (100), showing the 3-membered rings of $M(O,OH,H_2O)_6$ octahedra and PO_4 tetrahedra which constitute the basic subunits of each chain. The SO_4 groups are attached to the outer margins of the chains, where they receive the hydrogen bonds (dashed lines) that bridge the interchain gaps. The "interlayer" H_2O are represented as small black circles.

This ensures local charge neutralization and thus promotes the overall stability of the structure.

With regard to the underbonded oxide ions, the number and strength of H bonds to any given acceptor O atom should be proportional to the degree of underbonding of that atom. Specifically, the degree of underbonding increases in the order O8 ~ O2 ~ O3 $\ll$ O15 < O14 < O12, the first 3 atoms being moderately underbonded (valence sum = 1.8 v.u.) and the last 3 much underbonded (valence sum = 1.5 − 1.6 v.u.). Inspection of interatomic distances (Table 8) involving H atoms and the O atoms of OH and H_2O groups shows that, as expected, the members of the first group receive 1 or 2 H-bonds and have average

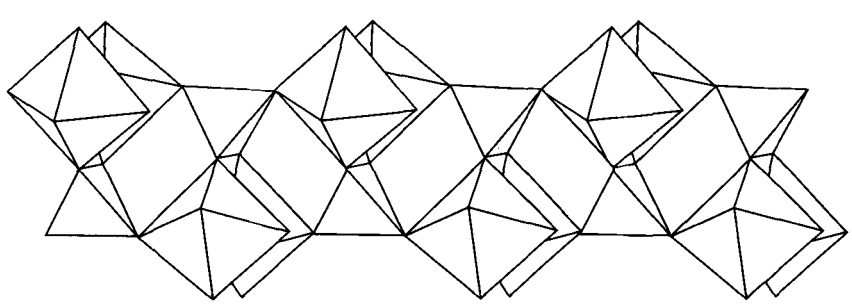

Figure 5. A polyhedral representation of 1 chain, showing the method of linkage of adjacent intrachain subunits. The peripheral SO_4 groups are omitted.

https://doi.org/10.1346/CCMN.1999.0470101 Published online by Cambridge University Press

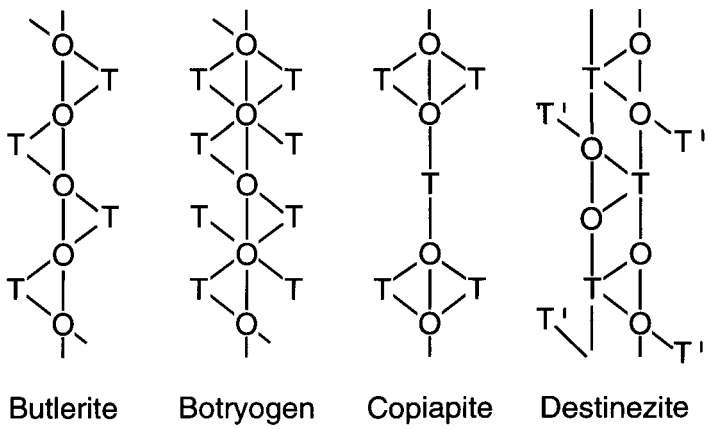

Figure 6. Schematic representations after Süsse (1971) of the chain structures in hydrated Fe sulfates containing 3-membered rings of 2 octahedra plus 1 tetrahedron. Symbols: O = $Fe(O,OH,H_2O)_6$, T = SO_4 (except for destinezite, where T = PO_4 and T′ = SO_4), line = a shared polyhedral vertex.

H . . . O and O–O distances of 2.02 and 2.81 Å, respectively, whereas members of the second group receive 2 or 3 H-bonds and have average H . . . O and O–O distances of 1.91 and 2.75 Å, respectively (excluding the weak O11w–H10 . . . O12 interaction). Thus, the more severely underbonded atoms receive stronger H-bonds, the bond strengths being inferred qualitatively from the distances O–O and H . . . O.

Interlayer Bonding

The layered aspect of the destinezite structure is defined by slabs of parallel chains separated by planes of interlayer water molecules, O11w. Hydrogen bonding involving O11w, O5w, O7h and O13w is the only mechanism by which adjacent slabs are bonded together (Figure 4). Atom O11w is a donor to underbonded oxide ligands of sulfate and phosphate groups in adjacent slabs through the configurations O11w–H10 . . . O12(S) and O11w–H11 . . . O3(P) and is also an acceptor from H_2O ligands of MX_6 groups through the configurations (M1)O5w–H6 . . . O11w and (M2)O13w–H12 . . . O11w. (Here the symbols in parentheses indicate the chain cations to which donor or acceptor oxygen atoms are bonded). The combined donor-acceptor role of O11w produces a coordination of this atom by 4 H atoms at the vertices of a distorted tetrahedron.

DIADOCHITE AND DESTINEZITE AS POSSIBLE SIGNIFICANT SOIL MINERALS

Well-crystallized destinezite most commonly occurs in reniform nodules several centimeters in diameter associated with clay minerals and other phyllosilicates. The nodules are aggregates of minute tabular crystallites, ranging in size from a few to a few tens of micrometers. At the type locality, destinezite nodules occur embedded in clay beds in a coal formation and are associated with minute crystals of quartz and mica (Cesàro 1885, 1897). Another typical locality is the Kurama Ridge in the Tokmak leucocratic zone of Uzbekistan (Moiseeva 1967, 1970), where the nodules occur in kaolinite and hydromica beds associated with gypsum and jarosite in sericitized volcanic rocks. Here the formation of destinezite is attributed to reaction of primary apatite with sulfate-bearing solutions derived from the decomposition of pyrite (Moiseeva 1967). The formation of destinezite from apatite (and perhaps other primary and secondary phosphates) and sulfate solutions derived from alteration of pyrite is perhaps the most frequently cited mode of formation for this mineral, and this pattern holds true for the Alum Cave Bluff occurrence.

The surface waters at Alum Cave Bluff are highly acidic, an observation consistent with laboratory ex-

Table 9. Empirical bond valences (v.u.).

	O1w	O2	O3	O4w	O5w	O6	O7h	O8	O9	O10w	O11w	O12	O13w	O14	O15	ΣV_c
M1		0.42	0.56		0.43		0.59	0.60		0.44	—					3.04
M2	0.40			0.39		0.63	0.58		0.63		—		0.46			3.09
P			1.26			1.27		1.20	1.27		—					5.00
S		1.39									—	1.52		1.58	1.62	6.11
ΣV_a	0.40	1.81	1.82	0.39	0.43	1.90	1.17	1.80	1.90	0.44	—	1.52	0.46	1.58	1.62	

Note: Bond valences for M1 and M2 are weighted averages for $(Fe_{1.81}Al_{0.19})$ and $(Fe_{1.73}Al_{0.27})$, respectively. All valences are calculated using the constants of Brese and O'Keeffe (1991).

https://doi.org/10.1346/CCMN.1999.0470101 Published online by Cambridge University Press

periments on similar rocks, which have yielded pH values as low as 2 (Jago 1989). The coexistence of gypsum and destinezite in an acidic, evaporitic environment at Alum Cave Bluff (and other localities) has implications for the possible formation of destinezite in soils under non-evaporitic conditions. The equilibrium represented by the reaction:

$$Ca_5(PO_4)_3(OH) + 8SO_4^{2-} + 6Fe^{3+} + 30H_2O = 5CaSO_4{\cdot}2H_2O + 3Fe_2(SO_4)(PO_4)(OH){\cdot}6H_2O + 2H^+ \quad [1]$$

lies to the right at Alum Cave Bluff, suggesting that hydroxylapatite in soil should react with a sufficient concentration of sulfate and ferric iron ions to produce destinezite plus gypsum. Under humid conditions the gypsum would be removed in solution.

The more stable fluorapatite should be more resistant to chemical attack, but the presence of Ca may provide a fluoride sink so that a second equation may be written:

$$2Ca_5(PO_4)_3F + 15SO_4^{2-} + 12Fe^{3+} + 60H_2O = CaF_2 + 9CaSO_4{\cdot}2H_2O + 6Fe_2(SO_4)(PO_4)(OH){\cdot}6H_2O + 6H^+. \quad [2]$$

If this reaction also proceeds to the right in the presence of sufficient concentrations of sulfate and ferric iron ions, then soil fluorapatite should be unstable and react to produce destinezite plus gypsum plus fluorite. As in the previous case, the gypsum would be removed in a humid climate. Acid conditions are required for this reaction in order to maintain a sufficient concentration of ferric iron ions in solution. Under conditions of higher pH, the concentration of ferric ions will be reduced to a small value by precipitation of ferric oxides (such as goethite and hematite), and both reactions will be driven to the left. Therefore, the formation of destinezite should be favored in soils having low pH values.

Although destinezite and diadochite have not been previously reported as soil minerals (Lindsay et al. 1989), P. B. Moore (personal communication 1995) has suggested that they may be significant in some soils, in part as repositories of inorganic phosphate. Indeed, the occurrence of destinezite in that role at Alum Cave Bluff suggests that additional occurrences may exist wherever the associated rocks have the appropriate mineralogical composition noted above. "Diadochite" is also a common alteration product of primary pegmatite phosphates in the zone of weathering, where it occurs as thin, discontinuous films and crusts in fractures in quartz. Soil scientists should be cognizant of the possible occurrence of diadochite/destinezite in soils where it is geochemically favored by the conditions defined above. At the hand specimen level where it is sufficiently abundant to be identified, it may appear to be little more than an obscure surface coating. Indeed, it is conceivable that diadochite is a minor, but not uncommon, constituent of some soils, its presence having gone undetected owing to the fact that its noncrystalline or poorly crystalline character and minute grain size inhibit its identification by the standard powder XRD techniques commonly used for studies of soil mineral assemblages.

ACKNOWLEDGMENTS

We thank Prof. A.-M. Fransolet for kindly providing a sample of destinezite from the type locality. We are also grateful to Dr. George Robinson for his initial identification of destinezite in Alum Cave Bluff samples.

REFERENCES

Ankinovich EA. 1958. Diadokhit iz vanadienosnikh slantsev Severo-Zapadnogo Karatau. Izv Akad Nauk Kaz SSR, Ser Geol, No. 3:79–83 [Chem Abstr 53:9910e].

Brese NE, O'Keeffe M. 1991. Bond-valence parameters for solids. Acta Crystallogr B47:192–197.

Cesàro G. 1885. Étude chimique et cristallographique de la destinézite (diadochite de Visé). Ann Soc Géol Belg, Mém 12:173–191.

Cesàro G. 1897. Description des minéraux phosphatés, sulfatés et carbonatés du sol belge. Mém Acad R Sci Lett Beaux-Arts Belg 53:1–136.

Chiari G, Ferraris G. 1982. The water molecule in crystalline hydrates studied by neutron diffraction. Acta Crystallogr B38:2331–2341.

Clark AM. 1993. Hey's mineral index: Mineral species, varieties and synonyms. London: Chapman & Hall. p 177–178.

Coskren TD, Lauf R. 1996. Secondary sulfates of Alum Cave Bluff, Great Smoky Mtns., Tennessee. Rocks and Minerals 71:192–193.

Fleischer M, Mandarino JA. 1995. Glossary of mineral species 1995. Tucson, AZ: The Mineralogical Record. p 52–53.

Földvári M, Nagy B. 1985. Diadochit és desztinezit Mátraszentimréről. Földt Közl 115:123–131 [Chem Abstr 107: 158449r].

German LD. 1956. O destinezite v zone okisleniya kolchedannogo mestorozhdeniya Blyava na Yuzhnom Urale. Zap Vses Mineral O-va 85:574–577 [Chem Abstr 51:7957i].

Hausen D. 1962. Cited as a private communication on Powder Diffraction File Card 12–209.

Hintze C. 1933. Handbuch der Mineralogie, vol 1, Part 4 (2nd Half). Berlin: Walter De Gruyter. p 745–756, 1071–1074.

Jago WK. 1989. Geochemical assessment of acid drainage in the Blue Ridge Province of Tennessee and North Carolina [M.S. thesis]. Knoxville, TN: Univ of Tennessee. 117 p.

Jarkovský J, Čičel B. 1958. Výskyt diadochitu v Banskej Belej. Geol Práce, Zprávy 13:97–104 [Chem Abstr 53:994i].

Larsen ES. 1921. The microscopic determination of the nonopaque minerals. US Geol Surv Bull 679:67.

Lindsay WL, Vlek PLG, Chien SH. 1989. Phosphate minerals. In: Dixon JB, Weed SB, editors. Minerals in soil environments. Madison, WI: Soil Science Society of America. p 1089–1130.

Mereiter K. 1979. Die Kristallstruktur von Mangan (III)-hydroxid-sulfat-Dihydrat, $Mn(OH)SO_4{\cdot}2H_2O$. Acta Crystallogr B35:579–585.

Moiseeva MI. 1967. O nakhodke destinezita v Kuraminskom Khrebte. Dokl Akad Nauk Uzb SSR, No. 9:45–47 [Chem Abstr 68:14731e].

Moiseeva MI. 1970. Mineralogiya kori vivetrivaniya Kuraminskogo khrebta i usloviya ee obrazovaniya. Zap Uzb Otd Vses Mineral O-va, No. 23:46–54 [Chem Abstr 75: 119980h].

North ACT, Phillips DC, Mathews FS. 1968. A semi-empirical method of absorption correction. Acta Crystallogr A24: 351–359.

Palache C, Berman H, Frondel C. 1951. The system of mineralogy, vol II. New York: J. Wiley. p 1011–1013.

Scordari F. 1981. Fibroferrite: A mineral with a $(Fe(OH)(H_2O)_2SO_4)$ spiral chain and its relationship to $Fe(OH)SO_4$, butlerite and parabutlerite. Tschermaks Mineral Petrogr Mitt 28:17–29.

Süsse P. 1968. Die Kristallstruktur des Botryogens. Acta Crystallogr B24:760–767.

Süsse P. 1971. Kristallchemie und Klassifikation der natürlichen Ferrisulfate. Fortschr Mineral 49:119–121.

Süsse P. 1972. Crystal structure and hydrogen bonding of copiapite. Z Kristallogr 135:34–55.

van Tassel R. 1985. Minéraux phosphatés secondaires (vashegyite, destinézite, wavellite, crandallite, phosphate der fer) à Haut-le-Wastia, province de Namur (Belgique). Bull Soc Belge Géol 94:19–27.

Veselý V. 1922. Chemické složení nerostů z Chvaletic a Litošic. Rozpravy České Akad, Tr II 31:No 9 [Chem Abstr 18:34].

Walker N, Stuart D. 1983. An empirical method for correcting diffractometer data for absorption effects. Acta Crystallogr A39:158–166.

(Received 21 February 1997; accepted 11 May 1998; Ms. 97-019)